Paleomagnetic full vector record of four consecutive Mid Miocene geomagnetic reversals

J. Linder, R. Leonhardt

Accepted Manuscript

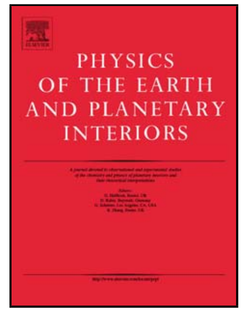

Title: Paleomagnetic full vector record of four consecutive Mid Miocene geomagnetic reversals

Authors: J. Linder, R. Leonhardt

PII: S0031-9201(09)00156-3
DOI: doi:10.1016/j.pepi.2009.07.013
Reference: PEPI 5188

To appear in: *Physics of the Earth and Planetary Interiors*

Received date: 31-7-2008
Revised date: 14-7-2009
Accepted date: 16-7-2009

Please cite this article as: Linder, J., Leonhardt, R., Paleomagnetic full vector record of four consecutive Mid Miocene geomagnetic reversals, *Physics of the Earth and Planetary Interiors* (2008), doi:10.1016/j.pepi.2009.07.013

Paleomagnetic full vector record of four consecutive Mid Miocene geomagnetic reversals

J. Linder ⋆, R. Leonhardt ⋄

⋆ *Department for Earth and Environmental Sciences, Ludwig-Maximilians-University, Munich, Germany*

⋄ *Institute for Geophysics, Montanuniversität Leoben, Austria*

Abstract

Seventy Mid Miocene lava flows from flood basalt piles near Neskaupstadur (East Iceland) were sampled, which provide a quasi-continuous record of geomagnetic field variations. Samples were collected along the Profile B of Watkins and Walker (1977), which was extended about 250 m farther down in a neighboring stream bed. Published radiometric age determinations (Harrison et al., 1979) range from 12.2 to 12.8 Ma for the sampled sequence. Four reversals were recorded in this profile, with 18 transitional lavas found within or between 17 normal and 30 reversed polarity flows. The large amount of transitional lavas and the large virtual geomagnetic pole dispersion for stable field directions are noteworthy as such features are commonly observed in Icelandic lavas and manifest in a far-sidedness of the average VGP. The reason for this characteristic, which could be related to an anomaly beneath Iceland, a global field phenomenon, local tectonics, and/or non-horizontal flow emplacement, is scrutinized. Non-horizontal flow emplacement is likely in volcanic environments particularly if the sampled lavas are located on the paleoslopes of a central volcano.

Preprint submitted to Elsevier Science *14 July 2009*

From the difference of the observed paleomagnetic mean directions to the expected directions assuming a geocentric axial dipole (GAD), a paleoslope which would explain the observed difference was calculated numerically. The obtained dip and dip direction point consistently to a possible volcanic extrusion center of the lavas. The determined paleodip, however, proved to be significantly too high compared to the usual slope of a central volcano, suggesting further reasons for deviations from the GAD. Other datasets of this age from Europe also show enhanced VGP dispersion, suggesting further contributions of geomagnetic origin for this observation. Basically all reversal paths move across the Pacific. Transitions were identified as belonging to C5An.1r - C5Ar.3r based on the Astronomically Tuned Neogene Timescale (Lourens et al., 2004). We selected 122 samples for paleointensity measurements using a modified Thellier method including tests for alteration and multidomain bias. 85 of the measured samples yielded data of sufficient quality to calculate paleointensities for 26 lava flows. The average paleointensity for stable field directions was 23.3 μT, whereas the intensity drops to a minimum of 5.8 μT during field transitions. The stable field intensities represent only about half of the present day field. The saw-tooth pattern of intensities, which is characterized by a sharp increase of intensity directly after a reversal and then followed by a gradual decrease towards the next reversal, was not found in this study.

Key words:

Paleomagnetism, absolute paleointensity, Eastern Iceland, Mid Miocene, Geomagnetic reversals

Email address: julia.linder@geophysik.uni-muenchen.de (J. Linder ⋆).

1 Introduction

The Earth's magnetic field has changed its polarity many times in the past. It is not known in detail how the geomagnetic field behaves during a reversal, but many results show a decrease of field intensity, likely related to a decreased dipole component, and multipole components, which become stronger (e.g. Merrill and McFadden, 1999; Leonhardt and Fabian, 2007). Detailed records of transitional fields were mostly obtained from sediments. In the work of Clement (1991), Tric et al. (1991) and Laj et al. (1991) the transitional VGPs were predominantly found within two approximately antipodal longitudinal bands across America and Asia. Some theories state the existence of this preferred longitudes of the virtual geomagnetic poles (VGPs) due to local flux concentrations of radial components and lower temperatures at the CMB. However, other studies (Prévot and Camps, 1993; Langereis et al., 1992; Leonhardt and Fabian, 2007) could not confirm these preferred longitude sectors. Beside geomagnetic reversals, the field behavior during stable polarities is subject of detailed research. The field's intensity was found to follow an asymmetric saw tooth pattern, which is characterized by a decrease before reversals and a large sudden recovery after the polarity change (Valet and Meynadier, 1993). However, remanences in sediments are often affected by post-depositional reorientation and the magnetic torque acting on the particles may not be sufficient to orient them properly (Tauxe, 1993). Furthermore the remanence acquisition can also be severely delayed (Roberts and Winklhofer, 2004), if sedimentation rate is low. In contrast to sediments, volcanic rocks record a geologically instantaneous field (Prévot et al., 1985) and provide the possibility to determine absolute paleointensities. Unfortunately, volcanic activity is usually very short lived and sporadic. Therefore, magnetic measurements at volcanic sequences are often of weak temporal resolution and cover only short time intervals.

Exeptional long time inervals, however, have been found particularly in Iceland (Watkins and Walker, 1977) and Kerguelen Archipelago (Camps et al., 2007). The flood basalt piles in East Iceland, cover an enormous age range and they are highly suitable for paleomagnetic measurements due to the extrusion of one lava flow per 10 kyr, a mean extrusion rate which is assumed to be quite homogenous in the lower part of the pile (Watkins and Walker, 1977). Previous paleomagnetic projects in Eastern Iceland are the work of Watkins and Walker (1977) in Neskaupstadur and of Kristjansson (1995) at the neighboring peninsula. Watkins and Walker (1977) magnetistratigraphically correlated 700 successive lavas in the flood basalt pile, ranging from 13.6 to 2.0 Ma in age. Herrero-Bervera et al. (1999) repeated the Watkins and Walker profiles C and D (12.09-10.21 Ma) for a more detailed examination of transitional lava flows and reversal paths. In this study, profile B of Watkins and Walker (1977) was repeated and extended 200 m farther down to determine the directional behavior and absolute paleointensity variation across geomagnetic field reversals, as well as to analyze the full vector record during stable polarity intervals.

2 Geological setting and field work

Samples were taken from lava flows of the flood basalt pile mountain Nipokollur (65.157 °N, 13.656 °W) near Neskaupstadur, Eastern Iceland. These flood basalts are well stratified and dip towards the active zone due to spreading

(Walker, 1974). The regional dip in the flood basalts piles of Neskaupstadur varies from 8 ° at sea level to 4° at mountain summits. On average this regional dip decreases with 1-1.5 ° per 200 m altitude (Kristjansson, 1995) due to down-dip thickening of the lava flows (Walker, 1964). The average accumulation rate of the basalt piles of 700-1000 m per Myr is decreasing with altitude. Due to intensive erosion only 1200 m altitude of the originally 10 km thick plateaus is left today (Krafft, 1984). Glaciers created the fjords in the Quaternary (Kristjansson, 1995), leaving outstanding outcrops of the basalt piles. In principle, we followed profile B of Watkins and Walker (1977) (see Fig. 1), but extended it farther down to 199 m altitude (original profile was down to 550 m). With a total of 70 lava flows an altitude of about 500 m was covered. Within the sampled profile some dykes (about 2 m wide) came close to the sites. A minimum distance of 9 m was always kept to prevent a thermally induced magnetic overprint of the dyke. Below site 20 we had to proceed the profile in a neighboring stream bed, as a very broad dyke crosses the outcrops of our section and the minimum distance could not be maintained anymore. Within the section also pillow lavas were found, which presumably formed in some shallow temporary ponds (Walker, 1974). Individual lavas were distinguished by red beds or paleosoils as well as top and basal breccia of the flow. Six samples per site with a diameter of one inch (2.54 cm) were cored using a gasoline-powered portable drill with a water-cooled diamond bit. Whenever possible samples were drilled horizontally distant and in the lower third of a lava flow in order to avoid any reheating from later flows above.

3 Methods and Results

3.1 Rock Magnetism

For a preselection and eligibility testing of the samples for paleointensity determinations, rock magnetic measurements were carried out for one sample per site, including isothermal remanent magnetization (IRM) aquisition, back field curves and hysteresis measurements with a peak field of 900 mT and thermomagnetic measurements with a peak temperature of 700 °C at the variable field translation balance (VFTB) of Petersen instruments. Hysteresis measurements revealed that most of the samples are within the PSD range and cluster along the SD-MD mixture lines (Dunlop, 2002) (see Fig. 2). Thermomagnetic results are discussed in the following together with ore microscopy. Furthermore, we performed measurements of the anisotropy of magnetic susceptibility on a representative part of the collection to test for the possibility of anisotropy bias in paleointensity determination and to analyze the flow directions of the lava flows (Henry et al., 2003). All investigated samples are found to be isotropic, based on anisotropy values well below 1.5%.

3.2 Thermomagnetic curves and ore microscopy

Samples were classified into four groups based on microscopy and thermomagnetic experiments (see Fig. 3). Ore microscopic observations of 14 samples helped to determine the oxidation state of the magnetic rock and to identify the remanence carriers.

Group 1 samples (5 % of samples) show two Curie temperatures, one around

200°C and the other at 450°C. The lower Curie temperature is likely related to unoxidized regions in the titanomagnetites as shown in the ore microscopy picture. Accumulation of ferrofluid along cracks in these titanomagnetites suggests a secondary maghemitization, which is responsible for the second Curie temperature.

The dominant Curie temperature of group 2 (10 %) range between 250°C and 430°C. As shown in the microscopy picture, cracks are abundant in the magnetic minerals, likely induced by shrinking during low temperature oxidation. Therefore this magnetic phase is interpreted to be titanomaghemite. Skeletal and cruciform structures can also be observed, which are a result of late crystallization of the TM into an already firm matrix, typical for tholeiitic magmas (Carmichel et al., 1960). Additionally, a minor ammount of high temperature oxidized grains are present, carrying a primary magnetization above 450°C.

Judging from ore microscopy, group 3 samples (25 %) are very similar to group 2 samples, except for the fact that the presence of a high temperature oxidized titanomagnetite is clearly visible in the thermomagnetic curve.

Samples of group 4 (60 %)(Fig. 3) are characterized by single Curie temperatures between 500° and 580°C. Beautiful exsolution lamellae were found in these samples, indicating high temperature oxidation. Highly oxidized phases are relatively insensitive to further oxidation under laboratory conditions, which is an excellent qualification for any paleomagnetic analysis. Only samples from sites, where this behavior was observed, were subjected to paleointensity determinations.

3.3 Paleodirections

NRM measurements were carried out in the magnetically shielded laboratory of the LMU in Niederlippach. A cryogenic magnetometer for the weaker magnetized samples and a spinner magnetometer for the stronger ones were used to determine the samples' remanences. Half of the samples per site were subjected to alternating field demagnetization (up to 200 mT) and the other half was thermally demagnetized (up to 600 °C) with at least 14 steps. Measurements of the susceptibility with a Geofyzika KLT-3 minikappa bridge after every heating step helped to recognize the onset of chemical alteration of the thermally treated samples. Typical demagnetization diagrams for normal, reversed and transitional directions are shown in Fig. 4a. For over 90 % of all samples of Neskaupstadur the orthogonal projection is characterized by a stable directional component. Despite their age most samples only carry a minor viscous overprint, which is demagnetized between 100 and 150 °C (see Fig. 4). For some samples principle component analysis could not be applied. Those directions were evaluated using great circle techniques (McFadden and McElhinny, 1988) (see Fig. 4b). Few samples contain a major magnetic overprint or a unstable direction with a too small unaffected NRM to be evaluable (see Fig. 4c). Only samples with a confidence cone $\alpha_{95} < 12°$ and a concentration parameter $k > 40$ (calculated using Fisher (1953) statistics) were included into further evaluation of the paleodirections.

Tilt corrections had to be applied to the dataset, as the center of Iceland subsided due to spreading effects and the weight of the glaciers and extrusions. Thus, the flood basalt pile near Neskaupstadur has an regional tilt of about 4-8° to 264°W. In most previous studies (Watkins and Walker, 1977; Kristjansson, 1995; Herrero-Bervera et al., 1999) it is assumed that the flood basalts flow over very far distances with negligible slope and were emplaced subhorizontally. Therefore a tilt correction to horizontal is applied to the Tertiary basalt piles in Eastern and Western Iceland with a dip direction pointing towards the central ridge and a dip varying with altitude due to down-dip thickening. The same approach is used here for initial analysis and its validity will be discussed below. By linear interpolation the dip values of the lava flows were calculated to vary from 7 ° for the sites JD-10 (150-300 m), 6 ° for the sites 11-25 (300-450 m), 5 ° for the sites 27-45 (450-600 m) to 4 ° for the uppermost sites 46-64 (600-761 m).

Four reversals were found within the section (see Fig. 5) with the transitional directions of the sites 51-46B (denoted reversal D below), 36-29 (reversal C), 16-14 (reversal B) and 11-05(reversal A). The sites 62-58 are assumed to represent an excursion, the sites 00-JD could indicate the termination of a preceding reversal. Using a cut-off colatitude for transitional lavas of 41.3 ° (McElhinny and McFadden, 1997) we found 18 transitional, 30 reversed and 17 normal polarities in the section. From 6 sites no reliable paleodirection could be derived. At a first glance the inclinations represent the expected values of a GAD pretty well (see Fig. 5). The declination scatters, but this is a typical feature at high latitudes.

Numerous dykes are found within the lava pile of eastern Iceland. In our profile, the minimum distance between dyke and sampling locality was 9 m (for the sampling spot at flow JD). In order to identify any possible magnetic overprint by later intrusion of this 5 m thick dyke, this dyke was sampled as well (site DY). Different directions between dyke and lava flow indicate that his dyke did not affect the remanence at our our sampling spot. The possible influence of dyke reheating was also investigated by a contact test close to site 13. This lava flow is crossed by a relatively thin dyke (≈3m). Four samples were taken from the dyke itself, another four in increasing distances (0.7 to 2.6 m) from the dyke. All samples show a similar directed and relatively strong overprint up to 370°C. Above this temperature distinctively different directions are observed between dyke and lava flow, already at closest distance of 0.7 m. Most dykes along the sampled profile are of similar or less width compared to the dyke crossing the section at site 13. Thus the minimum distance of more then 9 m to the dyke, which was kept for all sites, is sufficient to prevent sampling of reheated rocks.

3.4 Paleointensities

The intensity of the TRM in the flood basalts depends on the amount of magnetic minerals, their composition, grain size and grain shape, the decay of the magnetization with time and, of course, the ancient magnetic field. For the paleointensity measurements in this study the MT4 method (modified Thellier type four, containing alteration (CK), tail (TR) and additivity checks (AC)) (Leonhardt et al., 2004) was used. The laboratory field inside the shielded furnace, applied during heating and cooling, was chosen to be 30 μT, about half of the present day field, because of the high amount of transitional lavas and due to the presumed Miocene dipole low (Prévot et al., 1985). The samples of 8mm diameter and 7mm length were magnetized along the z-axis and kept in the same position within in the furnace during all temperature steps to minimize bias from temperature gradients and field variations. Due to the small sample size slightly larger orientation errors occur in the x-y plane, leading to more scattered horizontal components on the orthogonal projections. Paleointensity determinations, however, are unaffected. ThellierTool4.11 (Leonhardt et al., 2004) was used to analyze the paleointensity determinations. All analyzes are characterized by origin pointing stable directional component in agreement with its directional analysis, NRM fractions f above 30% (average 73%), at least 5 successive data point, quality factors q above 2.3 (average 15.8), minor alteration contribution ($< 10\%$) determined both from the individual check differences and from the cumulative difference, and finally, the absence of any significant MD contribution as tested by tail checks ($\delta t^* < 5\%$ below the maximum unblocking temperature) and additivity checks. For a determination of a site mean value, only sites with more than two eligible samples were accepted. If more than two successful determinations are available for a site, then a weighted mean of the paleointensity and its uncertainty was calculated using the quality factor q (Coe et al., 1978) in order to emphasize intensity determinations of higher quality. For six sites only 2 determinations were successful, thus,the maximum possible uncertainty is given there. Tab. 2 summarizes the paleointensity results for the all measured samples. Magnetomineralogical changes during heating are the main reason for rejecting individual measurements. For some weakly affected samples corrections for these alterations were applied (Valet et al., 1996) using the cumulative alteration difference if any significant contribution from MD remanence could be excluded based on tail checks. Furthermore, check corrected samples (for an explanation of the cumulative alteration difference see Leonhardt et al. (2004)) were only included if additivity checks then fit the expected pTRM values suggesting a preservation of essential TRM properties despite laboratory magnetomineralogical changes and if at least one value per site could be determined without corrections. One third of the collection was analyzed by applying the correction technique. The mean paleointensity of 23.3 μT for stable polarities across the section is very low. The values including reversals range from a minimum of 5.8 μT at site 32 to 22.8 μT at site jb and their average with 13.3 μT is about half of the non-transitional periods.

4 Discussion

4.1 Stable polarity fields

Magnetostratigraphic correlation. Due to their stratigraphic succession, the flood basalt piles in Eastern and Western Iceland provide an independent geomagnetic timescale back to 13 Myr ago (Harrison et al., 1979), which can be correlated with marine magnetic anomalies. At first we compared our data to the results of profiles A and B of Watkins and Walker (1977), which are based on two measurements for each directional unit. Based on flow descriptions, similar altitude, and their position relative to pronounced red beds, some lava flows (see Table 1) could be unambiguously correlated to profile B of Watkins and Walker (1977). Above these flows a direct flow-to-flow correlation between Watkins and our work is not possible, because of slightly different sampling routes. Based on altitude measurements, however, both profiles can be compared and paleodirectional comparisons yield mostly similar results, although some differences in particular for transitional directions are also observed. Watkins sampled older lava flows down to sea level in a different stream bed some hundred meters to the east, denoted profile A (Watkins and Walker, 1977). Based on directional results, our data shows similar prominent features as a composite A+B section of Watkins and Walker (1977). One discordance concerns the 12d chron (Opdyke, 1972). Instead of a normal polarized site at this altitude as stated by Watkins and Walker (1977) we found a transitional VGP in the northern hemisphere. The normal directions could have been missed due to gaps (35m gap between site 10 and 11 and 60m between site 13 and 14) in our section. Another possibility would be the insufficient demagnetization in the previous work and thus, no 12d normal chron in the previously sampled section. Correlation to global timescales like the Astronomically Tuned Neogene Timescale ATNTS2004 (Lourens et al., 2004)(see Fig. 7) and radiometric dating of overlying and underlying profiles (McDougall and Schmincke, 1976; Harrison et al., 1979) give an age ranging from 12.2 to 12.8 Ma for the section, which is within the marine anomaly 5A. Based on this correlation the sampled section ranges from C5Ar.2r to C5An.1r.

Deviations from GAD field. A positive class B reversal test confirmed that the mean values of the normal and reversed polarity data show a good antipodality, indicating that no overprints, insufficiently removed secondary components or rotations falsify the VGPs. Although statistically not significant as the uncertainty ellipse includes the geographic pole, the average normal and reversed VGPs yield a slight right-handedness. Such right-handedness, however, can be observed in data from all over Iceland, independent of age and location (Kristjansson and Jonsson, 2007). As the right-handedness is independent of the location in Iceland and found in Eastern and Western Iceland, neither rotational effects nor relocalization due to spreading can be the cause. Some suggested possible explanations are a magnetic anomaly beneath Iceland (Kristjansson and Jonsson, 2007), maybe connected to the plume, or a persistent non axial-dipole field. All VGPs within the cut-off colatitude of 41.3° (McElhinny and McFadden, 1997) were used to determine the VGP scatter around the spin axis. McElhinny and McFadden (1997) proposed a angualr standart deviation of 20.2° for latitudes between 60° and 70° for the last 5 Myr. In this study we determined a a slightly enhanced between site angular standard deviation of 23.2° with upper and lower confidence limits of 30.2° and 18.9° (Cox, 1969).

The VGP latitudes in this study show a tendency to decrease from the mountain tops to the sea level . However, as will be shown in the following, these low VGP latitudes are an artefact due to the applied dip correction based on the assumption of horizontal emplacement of the lavas. If there was an initial topography like central volcanoes, which can have a slope up to 10°, then the flood basalts already had an initial dip during deposition and correction towards horizontal emplacement falsifies the result. Also the down-dip thickening (Walker, 1964) of the lava flows suggests an initial dip. To determine this paleoslope, which would explain the low VGP latitudes (see Fig. 8), the magnetic vector v_{GAD}, which would be derived from a GAD, was rotated to the measured vector v_{measured}. The paleodip and paleodip direction describing this rotation were found numerically.

For a determination of the measured vector v_{measured} the in situ mean directions were determined for each group of samples, which represent a polarity chron, to randomize the effects of paleosecular variation (see Fig. 8). VGPs from group one do not cluster very well, presumably an effect of the ending of a preceeding reversal. Group two only contains three sites, which is not enough to average out paleosecular variation. The groups three, four and five give good mean directions. However, sites 59-61 were not included into the calculation of the mean direction of group five, because of their excursional character. The v_{GAD} for the Neskaupstadur latitude consists of the expected inclination of $I = 77.0$ and declination of $D = 0$. This GAD vector was rotated about all possible paleodips ($0 - \frac{\pi}{2}$) and paleodip directions ($0 - 2\pi$). Thus, the expected $v_{\text{rotated GAD}}$ was determined. The norm of the vector subtraction $|v_{measured} - v_{rotated\ GAD}|$ was calculated and the minimum of the resulting array (minimum deviation of the two vectors) gives the best-fitting paleodip and paleodip direction (see Tab. 3 and Fig. 8).

The determined paleodip directions vary from 4° to 36° and are assumed to represent the flow direction of the flood basalts. By tracking back the direction where the lava flows came from (184-216°) Reydarfjordur central volcano, which is about 15 km away from Neskaupstdur, might be interpreted as possible extrusion source (see also Fig. 1).

However, the calculated paleodips of 19° to 41° are far too high for the slope of central shield volcanoes, which usually have a slope up to 10° (Schmincke, 2000). Thus, it has to be assumed, that the observed low VGP latitudes are not solely an effect of the paleoslopes and effects like a regional anomaly or a global field effect have to be taken into account. Remarkably, lower VGP latitudes than expected were not only found in Icelandic lava flows, but as well in the sedimentary datasets of Abdul Aziz et al. (2000) from Calatayud Basin in NE Spain (41.17°N, 1.28°E) and of Hüsing et al. (2007) from northern Italy (43.59°N, 13.56°E), which are of the same age. Despite the remancences of these sediments could be affected by inclination shallowing, all the data from different sites together suggest that the low VGP latitudes are most likely a global field effect. Nevertheless, for a more conclusive statement further datasets, particularly from the southern hemisphere, should be taken into account.

Paleointensity variation between reversals. For the two lowermost stable polarity intervals too few site were eligible for paleointensity determinations and thus no record of the intensity behavior could be obtained. During the polarity chron C5Ar.1r, the paleointensity builds up from site 18 with 8.5 μT to site 28 with 39.6 μT. Above site 35 a large scatter in intensity is observed. Instead of a slow increasing field intensity, the sites 39 (15.5 μT) as well as 43 (14.3 μT) represent low values for a normal polarity interval at high latitudes. The low intensity of site 43 can be interpreted as being related to the onset of the next reversal. During the last reversed polarity chron of this section (C5An.1r) the intensity reaches high values at site 55 (41.4 μT). Finally, a low paleointensity value (site 61) during C5An.1r is from a post-excursional site. Overall, the field is characterized by lower paleointensity values compared to the present day field. The VDM, calculated from the paleointensities of the inter-reversal sites, is $3.2 \pm 1.5 \cdot 10^{22} Am^2$. This is about half of the present dipole moment ($8 \cdot 10^{22} Am^2$) and even lower the previously published values for the Miocene ($5.9 \pm 0.8 \cdot 10^{22} Am^2$ (Leonhardt et al., 2000) and $6 \cdot 10^{22} Am^2$ (Juárez et al., 1998)). However, a VDM about $3.2 \cdot 10^{22} Am^2$ is close to the low-field level of $4 - 5 \cdot 10^{22} Am^2$ suggested by Shcherbakov et al. (2002) and Heller et al. (2003).

4.2 Transitional fields

Reversal paths. Although polarity transitions are geologically spoken so quick that it is difficult to find volcanic rocks that preserve a complete and accurate record, many transitional directions were found in the Nipukollur section. This is surprising looking at the relatively low extrusion rate of approximately one flow per 10 kyr. Fig. 9 shows the VGPs of the four transitions recorded in the sequence. VGPs of contemporary Spanish and Italitan data sets (Abdul Aziz et al., 2000; Hüsing et al., 2007) were compared to the results of this study. The oldest reversals C5Ar.2r-C5Ar.1n (see Fig. 9a) is a R-N transition. Prior to the reversed field direction some transitional poles are found east of Patagonia. A first transitional VGP from site 06 is found in Indochina. Sites 07 and 08 show transitional VGP offshore of South Americas west coast, before reaching the stable field direction in Scandinavia and Siberia. Comparisons to Watkins and Walker (1977) dataset of profile A indicate that site 06 is significantly older the sites 07 and 08. Therefore its field direction is assumed to be related to the C5Ar.2n normal chron and not the reversal C5Ar.2r-C5Ar.1n. No transitional directions are found in the Spanish data set (Fig. 9a). The N-R reversal B from C5Ar.1n to C5Ar.1r only contains one clearly transitional data point (site 15) in the middle of the Pacific close to Hawaii (Fig. 9b). Similar Pacific longitudes are observed in the European data which are, however, only weakly defined. A similar post-reversal swing in (Fig. 9b) is found in all three data sets. The R-N reversal C begins with a swing from Antarctica to Australia and back again (site 29). Such directional changes, sometimes referred to as precursors, occasionally accompany reversals (Valet, 2003). After this onset-excursion the VGP path spans straight across the Eastern Pacific and clusters (two lava flows) somewhat south of Hawaii. Such clusters could describe the stop-and-go behavior of reversals (Hoffman, 1992) or just be an effect of rapid extrusion of lavas. With East-West swings across Alaska the VGP moves to stable directions in Northern Canada and the Arctic. Similar directions as in the initial excursion and the post-reversal North American VGP cluster are observed in the Italian dataset, suggesting a dipolar dominance during these phases. The last C5An.2n to C5An.1r reversal D (see Fig. 9d) begins in the Arctic Ocean. Then the VGPs cluster near the Ninety-East-Ridge (site 47-49) and move on to Antarctica. Ten lava flows later a post-reversal excursion starts from Antarctica first in the direction of Cape Hope (site 58) but swings on to a near-equatorial VGP near French Polynesia (site 59) and moves on to south of Malaysia (site 60) and near Ninety-East-Ridge (site 61) before coming back to Antarctica. This post-reversal excursion seems to be similar to the termination loops found by Prévot et al. (1985), which show a trend to be anticlockwise in the southern hemisphere (Jacobs, 1984). With a last swing to the Amundsen Sea north of Marie Byrd Land (site 63 and 64) the sampled section ends. In almost all cases transitional directions can only be found in the final hemisphere, which can be interpreted as a general trend for the reversals to start pretty fast. This is in good agreement with the observation, that the termination paths are characterized by bigger loops and more intermediate directions than the onset path (Herrero-Bervera, 1986; Jacobs, 1984). A tendency for the Icelandic VGPs to be found in the Pacific (Kristjansson and Jonsson, 2007) can be affirmed with this study (Fig 9).

Intensity variations across a transition. Unfortunately, below site 18 only few sites were suitable for paleointensity measurements. A general trend of the intensities to decrease during the transitional states (Fig. 5) was found. During the reversals A and C the intensity even drops to values below 10 μT. These observations are in agreement with the common observation that transitions are accompanied by a substantial decrease in the mean intensity of the dipole field (see (Merrill and McFadden, 1999) and references therein). Remarkably the intensity also drops to below-transitional values during the C5An.1n chron. Pre- and post-reversal loops unfortunately yielded no paleointensity data, except for site 61, a post-excursional lava, which is characterized by a low intensity of 6.8 μT. Despite the high ratio of transitional lavas to non-transitional lavas, none of the four transitions provides a sufficient amount of data to give a detailed picture of the field's intensity behavior during a reversal. Most likely the frequency of the extrusion of lavas (approximately one lava per 10 kyr) was not high enough to provide a complete record of the field in transition. Furthermore, it is noteworthy that normal polarity results are characterized on average by lower intensity values than reversed polarity lavas.

5 Conclusions

The Watkins and Walker (1977) profile B in the flood basalt pile near Neskaupstadur, Eastern Iceland, was resampled and extended about 250 m farther down. The paleomagnetic record of this flood basalt section contains four geomagnetic field reversals. By correlating the directional data first to the data from Watkins and Walker (1977) and then to the astronomically tuned global timescale (Lourens et al., 2004) the section was identified to range from the reversed C5An.1r chron to the reversed C5Ar.2r and thus cover about 700 kyr of extrusions, approximately between 12.2 and 12.8 Myrs ago. Altogether 18 transitional lavas were identified, characterized by a VGP deviation from the geographic poles of more than 41.3°. The paleosecular variation is slightely enhanced in this section. The VGPs during the polarity chrons show a generally lower latitude than expected from a GAD field. Possible reasons for this deviation are related to a local anomaly beneath Iceland, a global field phenomenon and/or non-horizontal flow emplacement. Flood basalts normally flow over very large distances with negligible slope and thus, a bedding correction to the horizontal plane was carried out at first like it is done in most earlier studies. Using a numerical method the paleodip and paleodip direction, which could be responsible for the rotation of the VGPs expected from a GAD to the measured VGPs, were determined. The calculated flow direction points consistently towards a possible volcanic source, the Reydarfjordur central volcano. The calculated average paleodip (24.7°), however, seems to be too high for the slope of a central volcano, which usually have a slope of maximum 10°. Thus, non-horizontal flow emplacement cannot be the only reason for the observed VGP deviation. Other studies on Mid Miocene sediments of Italy and Spain (Hüsing et al., 2007; Abdul Aziz et al., 2000) also revealed large deviations from the GAD. Thus, the too low VGP latitudes from Iceland are most likely not a local, but a global field effect. This conclusion is also in accordance with the low mean paleointensity of 23.3 μT which represents about half of the present field intensity. The saw-tooth pattern (Valet and Meynadier, 1993), a fast rebuilding field after the termination of a reversal and a slow decay of the intensity during the polarity interval, was not found during the polarity intervals in this study. Contradicting the saw-tooth hypothesis, the paleointensities would even suggest an inverse feature: an increase of paleointensity for one investigated polarity interval(C5Ar.1r). The reversal paths of the VGPs run across the Pacific or Eastern Asia. Generally all paths are in the far-sided hemisphere outside of the proposed longitudinal bands. Other studies on Mid Miocene sediments (Hüsing et al., 2007; Abdul Aziz et al., 2000) also revealed far-sided reversal paths across the Pacific and E-Asia. Due to a low resolution the VGPs paths could not be compared in detail. Nevertheless, similar precursors and post-reversal loops were found in all studies, indicating a dipole dominance shortly before and after the reversals. Transitional lavas are characterized by a very low paleointensity, below 10 μT for two reversals. Altogether, the low intensities and low VGP latitudes suggest a larger influence of non-dipolar terms for Mid Miocene geomagnetic field than compared to today.

Acknowledgements

We thank Christian Verard, Annika Ferk and Stefan Eder for the help during the field trips. Leo Kristjánsson kindly provided the maps and had helpful suggestions for possible drilling sites. Hayfaa Abdul-Aziz and Silja Hüsing kindley gave access to their data from the Mid Miocene. We thank Pierre Camps and an anonymous reviewer for their helpful and constructive comments. The research was supported through grants from the Deutsche Forschungsgesellschaft (Wi1828/3-1 and So72/67-4).

References

Abdul Aziz, H., Hilgen, F., Krijgsman, W., Sanz, E., Calvo, J., 2000. Astronomical forcing of sedimentary cycles in the middle to late Miocene continental Calatayud Basin (NE Spain). Earth Planet. Sci. Lett. 177, 9–22.

Camps, P., Henry, B., Nicolaysen, K., Plenier, G., 2007. Statistical properties of paleomagnetic directions in Kerguelen lava flows: Implications for the late Oligocene paleomagnetic field. J. Geophys. Res. 112.

Carmichel, I. S., Turner, F., Verhoogen, J., 1960. Igneous Petrology. McGraw-Hill Book Company, Ch. Ferric-ferrous equlibrium in liquids, pp. 282–285.

Clement, B., 1991. Geographical distribution of transitional VGPs: Evidence for nonzonal equatorial symmetry during the Brunhes-Matuyama geomagnetic reversal. Earth Planet. Sci. Lett. 29, 48–58.

Coe, R. S., Grommé, S., Mankinen, E. A., 1978. Geomagnetic paleointensities from radiocarbon-dated lava flows on Hawaii and the question of the Pacific nondipol low. J. Geophys. Res. 83, 1740–1756.

Cox, A., 1969. Confidence limits for the precision parameter k. Geophys. J. R. astr. Soc. 18, 545–549.

Day, R., Fuller, M. D., Schmidt, V. A., 1977. Hysteresis properties of titanomagnetites: Grain size and composition dependence. Phys. Earth Planet. Inter. 13, 260–266.

Dunlop, D., 2002. Theory and application of the Day plot (M_{rs}/M_s versus H_{cr}/H_c) 1. Theoretical curves and tests using titanomagnetite data. J. Geophys. Res. 107, 10.1029/2001JB000486.

Fisher, R. A., 1953. Dispersion on a sphere. Proc. R. Soc. London A 217, 295–305.

Harrison, C., McDougall, I., Watkins, N., 1979. A geomagnetic field reversal time scale back to 13.0 million years before present. Earth Planet. Sci. Lett. 42, 143–152.

Heller, R., Merrill, R. T., McFadden, P. L., 2003. The two states of paleomagnetic field intensities for the past 320 million years. Phys. Earth Planet. Inter. 135, 211–223.

Henry, B., Plenier, G., Camps, P., 2003. Post-emplacement tilting of lava flows inferred from magnetic fabric study: the example of Oligocene lavas in the Jeanne dArc Peninsula (Kerguelen Islands). Journal of Volcanology and Geothermal Research 127, 153–164.

Herrero-Bervera, E., Walker, G. P. L., Harrison, C. G. A., Garcia, J. G., Kristjansson, L., 1999. Detailed paleomagnetic study of two volcanic polarity transitions recorded in eastern Iceland. Phys. Earth Planet. Inter. 115, 119–135.

Herrero-Bervera, E. & Theyer, F., 1986. Non-axisymmetric behavior of Olduvai and Jaramillo polarity transitions recorded in north-central Pacific deep-sea sediments. Nature 332, 159–162.

Hoffman, K. A., 1992. Dipolar reversal states of the geomagnetic field and core-mantle dynamics. Nature 359, 789–794.

Hüsing, S., Hilgen, F., Abdul Aziz, H., Krijgsman, W., 2007. Completing the Neogene geological time scale between 8.5 and 12.5 Ma. Earth Planet. Sci. Lett. 253, 340–358.

Jacobs, J. A., 1984. Reversals of the Earth's magnetic field. Adam Hilger Ltd, Techno House, Redcliff Way, Bristol.

Juárez, M. T., Tauxe, L., Gee, J. S., Pick, T., 1998. The intensity of the Earth's magnetic field over the past 160 million years. Nature 394, 878–881.

Krafft, M., 1984. Fhrer zu den Vulkanen Europas. Band 1: Allgemeines, Island. Ferdinand Enke Verlag, Stuttgart.

Kristjansson, L., 1995. New palaeomagnetic results from Icelandic Neogene lavas. Geophys. J. Int. 121, 435–443.

Kristjansson, L., Jonsson, G., 2007. Paleomagnetism and magnetic anomalies in Iceland. Journal of Geodynamics , doi:10.1016/j.jog.2006.09.014.

Laj, C., Mazaud, A., Weeks, R., Fuller, M., Herrero-Bevera, E., 1991. Geomagnetic reversal paths. Nature 351, 447.

Langereis, C., van Hoof, A. A. M., Rochette, P., 1992. Longitudinal confinement of geomagnetic reversal paths as a possible sedimentary artefact. Nature 358, 226–230.

Leonhardt, R., Fabian, K., 2007. Paleomagnetic reconstruction of the global geomagnetic field evolution during the Matuyama/Brunhes transition: Iterative Bayesian inversion and independent verification. Earth Planet. Sci. Lett. 253, 172–195.

Leonhardt, R., Heunemann, C., Krása, D., 2004. Analyzing absolute paleointensity determinations: Acceptance criteria and the software ThellierTool4.0. Geochem. Geophys. Geosys. 5, Q12016, doi:10.1029/2004GC000807.

Leonhardt, R., Hufenbecher, F., Heider, F., Soffel, H., 2000. High absolute paleointensity during a mid Miocene excursion of the Earth's magnetic field. Earth Planet. Sci. Lett. 184, 141–154.

Lourens, L., F.J., H., Laskar, J., Shackleton, N., Wilson, D., 2004. A Geological Time Scale 2004. Cambridge University Press.

McDougall, I., Schmincke, H.-U., 1976. Geochronology of Gran Canaria, Canary Islands: Age of shield building volcanism and other magmatic phases. Bull. Volcanol. 40, 57–77.

McElhinny, M. W., McFadden, P. L., 1997. Palaeosecular variation over the past 5 Myr based on a new generalized database. Geophys. J. Int. 131, 240–252.

McFadden, P. L., McElhinny, M. W., 1988. The combined analysis of remagnetization circles and direct observations in palaeomagnetism. Earth Planet. Sci. Lett. 87, 161–172.

Merrill, R. T., McFadden, P. L., 1999. Geomagnetic polarity transitions. Rev. Geophys. 37, 201–226.

Opdyke, N., 1972. Paleomagnetism of deep sea cores. Reviews of Geophysics and Space physics 10, 213–249.

Prévot, M., Camps, P., 1993. Absence of preferred longitude sectors for poles from volcanic records of geomagnetic reversals. Nature 366, 53–57.

Prévot, M., Mankinen, E. A., Coe, R. S., Grommé, S., 1985. The Steens Mountain (Oregon) geomagnetic polarity transition 2. Field intensity variations and discussion of reversal models. J. Geophys. Res. 90, 10417–10448.

Roberts, A. P., Winklhofer, M., 2004. Why are geomagnetic excursions not always recorded in sediments? Constraints from post-depositional remanent magnetization lock-in modelling. Earth Planet. Sci. Lett. 227, 345–359.

Schmincke, H., 2000. Vulkanismus. Wissenschaftliche Buchgesellschaft.

Shcherbakov, V. P., Solodovnikov, G. M., Sycheva, N. K., 2002. Variations in the geomagnetic dipole during the past 400 million years (Volcanic rocks). Izv. Acad. Sci. USSR Phys. Solid Earth, Engl. Trans. 38, 113–119.

Tauxe, L., August 1993. Sedimentary records of the relative paleointensity of the geomagnetic field: Theory and practice. Rev. Geophys. 31, 319–354.

Tric, E., Laj, C., Valet, J.-P., Tucholka, P., Paterna, M., Guichard, F., 1991. The Blake geomagnetic event: transition geometry, dynamical characteristics and geomagnetic significance. Earth Planet. Sci. Lett. 102, 1–13.

Valet, J.-P., 2003. Time variations in geomagnetic intensity. Rev. Geophys. 41, doi:10.1029/2001RG000104.

Valet, J.-P., Brassart, J., Le Meur, I., Soler, V., Quidelleur, X., Tric, E., Gillot, P.-Y., 1996. Absolute paleointensity and magnetomineralogical changes. J. Geophys. Res. 101 (B11), 25029–25044.

Valet, J.-P., Meynadier, L., November 1993. Geomagnetic field intensity and reversals during the past four million years. Nature 366, 234–238.

Walker, G., 1964. Geological investigations in eastern Iceland. Bulletin of Volcanology 27, 351–361.

Walker, G., 1974. NATO advanced study institutes series, Series C "Mathematical and Physical Series, Vol.11 Geodynamics of Iceland and the North Atlantic Area. Dordrecht, Reidel, Netherlands, Ch. The Structure of Eastern Iceland, pp. 177–188.

Watkins, N., Walker, G. P. L., 1977. Magnetostratigraphy of eastern Iceland. Am. J. Sci. 277, 513–584.

Fig. 1. **Left:** Sampled section as seen from the lighthouse of Neskaupstadur. Original profile B of Watkins and Walker (1977) indicated with the dashed line. The bold line marks the sampled section of this study. **Right:** Overview about previous paleomagnetic projects in Eastern Iceland (modified after Kristjansson (1995)).

Fig. 2. Day plot (Day et al., 1977) with mixture lines and boundary values according to Dunlop (2002). The samples cluster within the PSD range along the SD-MD mixture lines.

Fig. 3. Ore microscopy of samples from different rock magnetic groups: Group 1 contains 5 % of samples, group 2 10 %, group 3 25 % and group 4 60 %. Samples were covered with ferrofluid, except right picture of group 2 and the group 3 picture, which were examined under polarized light.

Fig. 4. Orthogonal projections of **a)** stable directions (Site 28 with reversed polarity, 46 with normal polarity and transitional JD transitional) and **b)** great circle (Site 46B) and **c)** rejected samples (Site 10)

Fig. 5. Paleodirections (declination and inclination) for each sampled site and absolute paleointensites for eligible sites versus altitude. The dashed lines denote the values expected from a GAD. The polarity log was generated using a cut-off colatitude of 41.3 ° (McElhinny and McFadden, 1997) with black for normal, white for reversed and grey for transitional lava flows. Reversals are numbered from A to D and polarity chrons denoted after global timescale (for correlation see Fig. 7.)

Fig. 6. Arai plots of site 12 and 25 together with orthogonal projections (black circle for declination and white circle for inclination). The dashed lines indicate the linear segment used for the calculation of paleointensity. Triangles denote the alteration check step, gray squares the additivity checks.

Fig. 7. Correlation of VGPs to the results of Watkins and Walker (1977) and to global timescales like the ATNTS of Lourens et al. (2004).

Fig. 8. Trend of VGPs to lower latitudes for the lower section of the profile. The grey line shows the bedding corrected data with the values of the regional tilt, the black line the in situ data. The mean VGP latitudes are calculated for each group of stable field directions and given in Tab. 3. The mean inclination is shown with a black star. Results of the MATLAB^{TM} calulations of the paleoslope are shown for each group. See text for more information.

Fig. 9. VGP paths projected on the globe for transitions in the Neskaupstadur/Nipukollur section. **a)** is the oldest R-N transition, **d)** the youngest N-R transition. The black star denotes the Icelandic site. The dashed grey lines is based on the Spanish data set, the pointed dark grey on the Italian data set.

Table 1: Directional results

Site	Altitude [m]	n/N	D_g [°]	I_g [°]	D_s [°]	I_s [°]	k	α_{95} [°]	F [μT]	VGP long. [°]	VGP lat. [°]	Pol.
64	761	6/6	268.2	-76.6	270.0	-80.6	490	3.0		204.6	-59.5	R
63	*740*	5/6	296.8	-72.9	305.5	-76.1	173	5.8		197.0	-44.8	T
62	*735*	5/6	198.5	-79.9	175.4	-80.8	49	11.1		154.8	-82.9	R
61	*731*	5/6	84.4	-50.7	84.4	-46.7	309	4.4	6.8	93.7	-22.9	T
60	*727*	4/5	66.2	-44.5	67.3	-40.7	326	5.1		106.3	-12.1	T
59	*718*	5/6	287.7	-49.5	289.8	-53.1	485	3.5		224.4	-22.6	T
58	*713*	6/7	159.6	-56.0	154.1	-54.8	90	7.1		26.5	-56.4	R
57	*703*	6/6	183.3	-74.2	169.1	-74.4	161	5.3		40.1	-83.4	R
56	*684*	4/6	174.6	-76.7	158.1	-76.2	230	6.1		78.4	-80.5	R
55	*681*	6/6	159.5	-83.1	133.5	-81.2	1919	2.5	41.4	121.6	-72.3	R
54	*675*	7/7	275.7	-80.9	284.5	-84.8	253	3.8		187.2	-60.9	R
53	*669*	7/7	265.4	-80.6	266.4	-84.6	487	2.7		191.1	-63.7	R
52	*660*	6/6	264.9	-76.8	265.3	-80.8	182	5.0	37.8	205.5	-60.9	R
51	*652*	6/6	225.9	-78.9	208.8	-81.7	328	3.7	25.1	203.1	-77.0	R
50	*629*	5/5	162.8	-67.2	153.9	-66.1	61	9.9		38.6	-68.3	R
49	619	5/6	111.4	-54.4	109.1	-50.8	72	9.1		74.0	-36.3	T
48	*616*	5/5	81.6	-47.3	81.8	-43.3	75	8.9		94.6	-19.4	T
47	612	4/4	75.5	-37.8	75.9	-33.8	150	10.3		96.8	-11.0	T
46B⋆	*609*	0/4										
46	606	6/6	356.7	80.0	334.8	79.4	235	4.4	23.3	291.6	79.5	N
45 (EB21)	598	6/6	355.8	75.2	337.4	74.5	47	9.9		244.5	79.0	N
44 (EB20)	*595*	6/6	44.6	69.0	34.5	72.6	308	3.8		84.1	72.3	N
43	*592*	6/6	47.0	75.0	32.0	78.6	55	9.1	14.3	49.2	77.1	N
42	590	6/6	25.9	79.2	358.7	80.8	176	5.1	32.5	343.0	83.1	N
41	586	5/5	348.4	75.9	329.9	74.6	237	5.0		253.8	76.0	N
40	*585*	6/6	313.8	77.4	300.5	73.7	278	4.0	26.0	273.0	63.0	N
39	583	6/7	351.6	60.9	342.8	60.3	496	3.0	15.5	197.0	64.2	N
38	571	5/5	340.6	73.1	326.0	71.3	76	9.1		243.1	71.2	N
37	566	6/6	309.1	75.3	298.4	71.4	226	4.5	25.5	268.7	59.8	N
36	562	6/6	347.5	52.7	341.1	51.9	101	6.7		195.1	55.4	N
35 (EB14)	551	4/5	349.8	50.0	343.9	49.4	755	3.3	10.4	190.2	53.7	N
34	540	0/6										
33	538	6/6	318.5	18.1	317.3	15.2	40	10.8		214.4	25.3	T
32 (EB10)	488	6/6	316.6	30.4	314.4	27.3	278	4.0	5.8	220.0	30.8	T
31	*472*	5/5	186.0	-62.8	176.2	-63.4	135	6.6	9.0	354.1	-69.7	R
30⋆	469	0/4										
29 (EB7)	463	5/5	44.1	-61.0	49.2	-57.0	133	7.1		126.8	-19.6	T
28 (EB6C)	460	5/6	204.3	-57.3	197.0	-59.5	354	4.1	39.6	316.6	-63.3	R
27	455	6/6	196.8	-59.4	188.5	-61.0	152	5.9		330.4	-66.4	R
25	443	6/7	203.3	-61.7	192.5	-64.1	154	5.4	25.0	320.8	-69.5	R
24	424	6/6	238.5	-76.2	221.6	-81.2	137	5.9	23.4	210.7	-73.7	R
23B	*420*	5/6	247.5	-65.4	242.6	-71.1	127	6.8		243.9	-59.1	R
23	418	5/5	186.3	-83.5	138.2	-82.2	123	7.4		128.5	-73.3	R
22	*410*	5/5	157.8	-51.1	151.0	-49.1	205	5.4		27.7	-50.5	R
21	406	4/6	156.2	-48.0	150.2	-45.9	179	6.9	14.8	27.4	-47.7	T
20	*401*	6/6	202.1	-76.6	175.9	-78.2	229	4.4		130.9	-87.3	R
19 (EB1)	*398*	6/6	177.2	-65.0	164.4	-64.7	95	6.9		18.4	-69.6	R
18	*388*	5/6	191.8	-64.4	179.2	-65.6	65	9.6	8.5	348.1	-72.6	R
17	*383*	6/6	200.9	-62.0	189.9	-64.2	60	8.7		325.8	-70.1	R
16	*378*	5/5	215.9	-75.6	193.1	-78.7	66	9.5		219.9	-84.0	R
15	*373*	6/6	338.2	8.5	337.4	6.8	74	7.8		191.7	26.2	T
14	*372*	6/6	49.7	70.6	37.0	75.2	206	4.7		69.7	73.6	N
12	*310*	6/6	62.6	67.6	55.5	73.1	42	10.4	7.3	64.2	64.0	N
11	*307*	6/6	80.8	77.6	77.8	83.6	97	6.8		16.5	64.8	N
10	*272*	0/7										
09	*269*	0/6										
08	*266*	3/3	267.7	-4.7	267.8	-11.7	194	8.9		255.8	-6.3	T
07	*265*	5/5	246.7	-19.1	245.8	-25.8	100	8.8		272.9	-22.4	T
06	*245*	6/6	60.1	18.3	59.0	24.7	55	9.3	6.8	99.7	24.5	T
05	*240*	6/7	276.5	-73.8	285.5	-80.5	123	6.1	15.7	199.1	-55.6	R
04	*235*	0/3										
03	*233*	7/7	281.6	-76.5	298.6	-82.9	97	6.2	16.1	188.8	-56.3	R
02	229	7/7	262.0	-70.0	261.0	-77.0	187	4.4	48.7	218.5	-58.4	R
01	*227*	8/8	254.0	-67.7	249.7	-74.5	99	5.6		231.1	-59.8	R
00	*222*	6/6	237.3	-68.5	226.1	-74.4	59	8.8		246.6	-69.1	R
JA	*217*	6/6	229.9	-51.7	224.0	-57.3	267	4.1	20.4	281.5	-52.8	R
JB	*214*	5/5	215.9	-41.8	210.7	-46.2	65	9.6	22.8	304.1	-47.7	T
JC	*209*	6/6	207.1	-32.9	202.9	-36.5	1385	1.8	14.3	316.6	-42.7	T
JD	*199*	5/6	211.3	-26.8	208.2	-30.9	167	5.9	22.0	311.3	-37.9	T
Dykes:												
13	*312*	5/8	19.0	44.8	13.3	47.1	52	10.7		147.0	52.2	N

Table 1: Directional results

Site	**Altitude [m]**	**n/N**	$\mathbf{D}_g$ [°]	$\mathbf{I}_g$ [°]	$\mathbf{D}_s$ [°]	$\mathbf{I}_s$ [°]	**k**	α_{95} [°]	**F** [μT]	**VGP long.** [°]	**VGP lat.** [°]	**Pol.**
DY	205	5/5			1.3	73.1	148	6.3		160.3	83.5	N

Directional results for all sampled sites. Altitudes (GPS-altitudes in normal fonts, italics for interpolated altitudes), n/N is the number of samples used for the calculation of the mean directions versus the number of samples treated, D_g and I_g denote declination and inclination in geographic coordinates, D_s and I_s the declination and inclination in stratigraphic coordinates, k and α_{95} indicate the concentration parameter and the confidence cone, F yields the weighted mean intensity of all suitable specimens of a site (see Table 2), VGP longitude and latitude give the coordinates of the virtual geomagnetic pole. The polarity of each flow are given with N for normal polarity, R for reversed and T for transitional (if the VGP latitude is below 48.7° (McElhinny and McFadden, 1997)). A * following the sample name denotes transitional lava flows, which could only be evaluated with great circle analysis. Based on flow descriptions, similar altitude, and their position relative to pronounced red beds, some lava flows could be unambiguously correlated to profile B of Watkins and Walker (1977). In this case the site name used by Watkins and Walker (1977) is given in parenthesis after our site name. Above and below these flows a direct flow-to-flow correlation between Watkins and our work is not possible, because of slightly different sampling routes. Comparison, however, is possible based on altitude measurements.

Table 2: Paleointensity results of Neskaupstadur section

Site	Alt.	n/N	Sample	T_{min}	T_{max}	N	f	g	q	w	F_i	σF_i	F	σF
64	761	0/2												
61	731	3/3	61-1*	400	580	7	0.79	0.72	24.8	11.1	7.2	0.2	6.8	0.3
			61-4*	400	580	7	0.79	0.71	21.6	9.6	6.4	0.2		
			61-5	430	610	7	0.85	0.75	11.0	4.9	6.9	0.4		
55	681	5/5	55-1	280	580	10	0.89	0.77	20.2	7.1	29.8	1.0	41.4	4.1
			55-2	100	520	15	0.48	0.84	6.0	1.7	47.2	3.1		
			55-3	310	520	7	0.37	0.80	4.6	2.0	37.5	2.4		
			55-4	100	490	13	0.44	0.88	39.1	11.8	45.4	0.5		
			55-5	200	490	8	0.46	0.82	10.6	4.3	47.1	1.7		
52	660	2/4	52-2*	200	460	7	0.33	0.80	2.6	1.2	29.7	3.0	37.8	6.3
			52-4	490	610	5	0.83	0.65	27.6	16.0	38.6	0.8		
51	652	3/3	51-2	370	610	9	0.90	0.76	18.3	6.9	21.4	0.8	25.1	1.9
			51-3*	400	610	8	0.86	0.82	20.2	8.3	27.6	1.0		
			51-6*	370	550	7	0.82	0.78	14.8	6.6	26.2	1.1		
49	619	0/2												
46	606	3/3	46-3*	490	610	5	0.66	0.58	13.3	7.7	19.4	0.6	23.3	1.5
			46-5	390	580	7	0.88	0.77	24.8	11.1	22.5	0.6		
			46-4	20	580	13	0.96	0.82	37.7	11.4	25.2	0.5		
43	592	3/3	43-2*	200	610	12	0.96	0.81	25.9	8.2	14.8	0.4	14.3	0.8
			43-3*	490	610	5	0.58	0.56	20.4	11.8	13.2	0.2		
			43-6	20	490	10	0.32	0.76	2.6	0.9	17.5	1.6		
42	590	3/3	42-3	20	520	16	0.67	0.90	32.0	8.5	31.7	0.6	32.5	2.6
			42-4*	190	520	11	0.77	0.88	5.1	1.7	42.8	5.7		
			42-6*	220	430	8	0.42	0.84	10.4	4.3	29.7	1.0		
41	586	0/3												
40	585	2/2	40-3	20	490	10	0.41	0.77	2.3	0.8	21.9	3.0	26.0	7.0
			40-6	100	460	8	0.30	0.83	2.4	1.0	29.9	3.1		
39	583	2/2	39-4	100	490	9	0.33	0.81	3.0	1.1	14.8	1.3	15.5	2.1
			39-6*	100	490	9	0.32	0.83	3.1	1.2	16.2	1.4		
38	571	0/3												
37	566	2/3	37-1	20	350	6	0.38	0.77	3.0	1.5	26.4	2.6	25.5	2.8
			37-6*	20	460	9	0.75	0.86	9.2	3.5	25.2	1.8		
36	562	0/3												
35	551	3/3	35-1	350	610	9	0.98	0.80	12.8	4.8	8.4	0.5	10.4	1.1
			35-3*	200	610	12	0.97	0.80	38.5	12.2	11.4	0.2		
			35-4*	250	520	8	0.56	0.76	3.4	1.4	7.1	0.9		
32	488	4/4	32-1	300	610	10	1.00	0.82	6.7	2.4	4.9	0.6	5.8	0.8
			32-3	220	580	12	0.85	0.77	11.4	3.6	6.6	0.4		
			32-4*	220	580	12	0.95	0.81	3.7	1.2	8.3	1.7		
			32-6	370	610	9	0.90	0.84	8.0	3.0	4.3	0.4		
31	472	3/4	31-2*	370	580	7	0.77	0.76	8.9	4.0	12.9	0.9	9.0	1.9
			31-4	370	580	7	0.75	0.71	14.4	6.4	8.3	0.3		
			31-5	370	520	5	0.41	0.61	7.0	4.0	5.7	0.2		
28	460	5/6	28-1	20	610	14	0.96	0.84	31.5	9.1	34.7	0.9	39.6	3.3
			28-2	200	430	6	0.31	0.77	6.1	3.0	42.6	1.7		
			28-3*	200	610	12	0.95	0.76	81.1	25.6	44.5	0.4		
			28-5	300	610	10	0.94	0.81	25.0	8.8	30.4	0.9		
			28-6*	350	610	9	0.99	0.78	7.8	2.9	36.1	3.6		
27	455	0/3												
25	443	4/4	25-3	350	610	9	0.93	0.81	20.9	7.9	25.4	0.9	25.0	0.2
			25-2	350	610	9	0.92	0.76	9.2	3.5	25.1	1.9		
			25-7*	430	610	7	0.78	0.70	10.9	4.9	24.8	1.3		
			25-5*	200	610	12	0.94	0.82	18.5	5.8	24.5	1.0		
24	424	3/4	24-1*	350	610	9	0.92	0.75	17.7	6.7	24.9	1.0	23.4	0.8
			24-4	20	350	6	0.62	0.76	3.6	1.8	22.9	3.0		
			24-6*	250	610	11	0.93	0.76	25.5	8.5	22.4	0.6		
23	418	0/3												
21	406	2/3	21-1	490	610	5	0.74	0.67	23.6	13.6	17.2	0.4	14.8	2.4
			21-2	390	610	8	0.89	0.72	31.7	13.0	13.1	0.3		
20	401	0/2												
18	388	3/4	18-1	310	520	7	0.36	0.76	5.8	2.6	10.7	0.5	8.5	2.0
			18-3	370	580	8	0.86	0.78	9.4	3.9	5.7	0.4		
			18-5*	130	280	6	0.33	0.75	4.0	2.0	12.1	0.7		
12	310	4/4	12-2	20	580	17	0.90	0.78	14.6	3.8	7.7	0.4	7.3	0.3
			12-3	220	550	11	0.84	0.76	8.1	2.7	6.8	0.5		
			12-4	340	520	6	0.48	0.65	4.3	2.1	8.1	0.6		
			12-6	220	550	11	0.84	0.74	18.7	6.2	7.1	0.2		
07	265	0/1												
06	245	3/4	06-2	490	610	5	0.82	0.69	29.8	17.2	8.0	0.2	6.8	0.7
			06-3*	300	610	10	0.92	0.61	28.3	10.0	6.7	0.1		
			06-4*	460	610	6	0.85	0.65	21.7	10.9	5.4	0.1		
05	240	2/2	05-4	20	490	10	0.35	0.74	2.5	0.9	18.6	1.9	15.7	4.4
			05-2	200	520	9	0.55	0.74	3.1	1.2	13.5	1.8		
04	235	0/3												

Table 2: Paleointensity results of Neskaupstadur section

Site	**Alt.**	**n/N**	**Sample**	T_{min}	T_{max}	**N**	**f**	**g**	**q**	**w**	F_i	σF_i	F	σF
03	233	2/4	03-1	20	550	12	0.58	0.86	10.9	3.4	13.6	0.6	16.1	2.7
			03-5*	430	610	7	0.87	0.69	16.4	7.3	17.8	0.7		
02	229	3/4	02-4*	100	580	16	0.94	0.78	25.3	6.8	53.2	1.5	48.7	2.8
			02-5*	310	550	8	0.91	0.73	12.6	5.1	46.9	2.5		
			02-7	370	580	7	0.87	0.78	23.0	10.3	44.7	1.3		
ja	217	4/4	ja-1	460	610	6	0.91	0.60	14.2	7.1	20.8	0.8	20.4	0.6
			ja-2*	490	610	5	0.78	0.56	48.3	27.9	20.4	0.2		
			ja-3	460	610	6	0.91	0.62	12.6	6.3	22.2	1.0		
			ja-4	490	610	5	0.86	0.57	14.4	8.3	18.2	0.6		
jb	214	4/4	jb-1	200	610	12	1.00	0.84	7.0	2.2	24.8	3.0	22.8	1.9
			jb-2	430	610	7	0.95	0.68	29.5	13.2	23.2	0.5		
			jb-3	490	610	5	0.88	0.57	14.8	8.6	18.0	0.6		
			jb-4	250	430	5	0.33	0.69	7.5	4.3	28.5	0.9		
jc	209	4/4	jc-1*	20	610	14	0.99	0.77	26.7	7.7	15.0	0.4	14.3	1.0
			jc-3	20	550	12	0.82	0.64	7.2	2.3	14.6	1.1		
			jc-4	460	610	6	0.74	0.68	8.8	4.4	10.7	0.6		
			jc-5*	250	490	7	0.40	0.80	4.7	2.1	16.6	1.2		
jd	199	4/4	jd-3*	490	610	5	0.70	0.67	20.8	12.0	19.1	0.4	22.0	1.4
			jd-4	250	550	9	0.84	0.81	32.5	12.3	22.4	0.5		
			jd-5	20	350	6	0.37	0.78	3.7	1.8	21.9	1.7		
			jd-6	490	610	5	0.88	0.67	10.4	6.0	26.4	1.5		

Site denotes the flow number and Alt their altitude in the profile. The success rate n/N is the number of successful measured samples per site versus the number of treated specimen. The sample name is extended by a superscripted star in case of check corrected analysis. T_{min} and T_{max} give the temperature interval used for the paleointensity calculations. N gives the number of successive data points in the used interval, f gives the used fraction of the NRM, g the gap factor and q the quality factor. The weighting factor is denoted w. F_i and σF_i give the paleointensity and its standard deviation for each single sample, F gives the weighted mean from the individual paleointensity measurements weighted with the quality factor q and the weighted standard deviation sigma F. If a site only contains two evaluable samples the minimum-maximum deviation was calculated instead of a weighted standard deviation.

Table 3
Paleodip and its direction. N denotes the number of flows used for the calculation.

Group (Sites)	N	Mean D/I	α_{95}	k	paleodip	paleodip direction
1 (jd-05)	9	229.6/-59.1	15.1	12.6	41	36
2 (11-14)	3	62.2/72.3	10.3	144.0	15	*107*
3 (16-31)	12	202.9/-68.6	6.0	53.0	34	14
4 (34-45)	10	358.1/76.3	6.1	63.2	3	4
5 (50-62)	8	233.8/-81.8	5.5	103.9	19	16
Mean					24.7	16.4

The dip direction of group 2 is printed italic, as only three sites contribute to the group mean direction. Therefore this result is assumed to be unreliable.

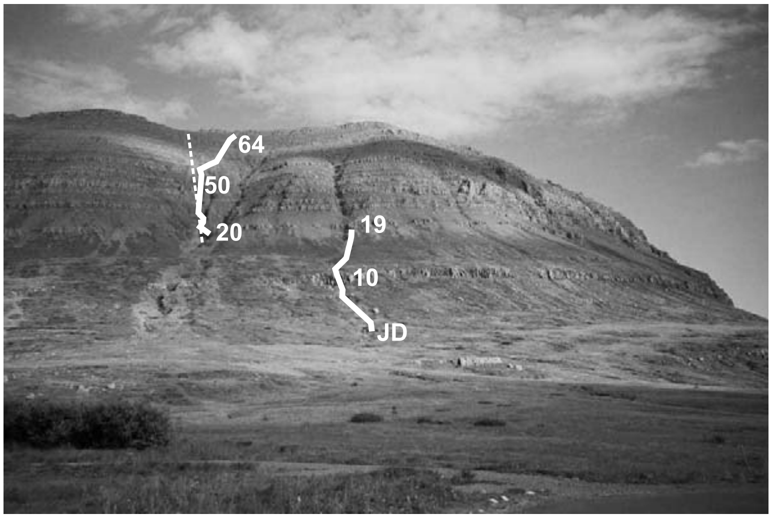
64
50
20
19
10
JD

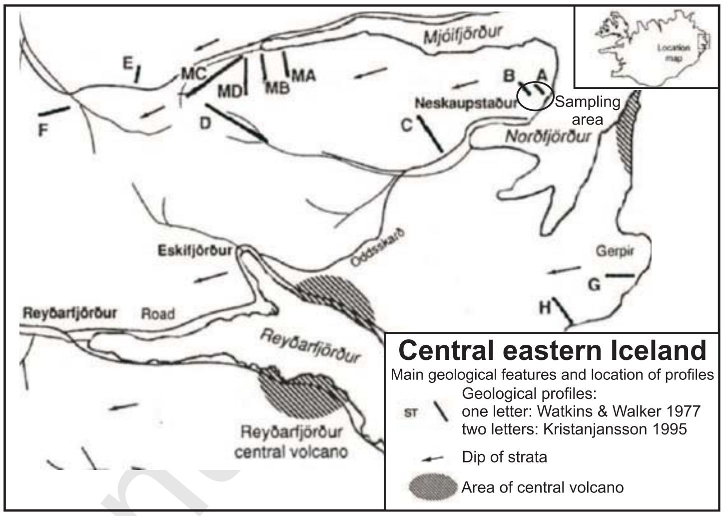
Mjóifjörður
E
MC
MD
MB
MA
B
A
Neskaupstaður
Sampling area
F
D
C
Norðfjörður
Eskifjörður
Oddsskarð
Gerpir
G
H
Reyðarfjörður
Road
Reyðarfjörður
Reyðarfjörður central volcano
Location map
Central eastern Iceland
Main geological features and location of profiles
Geological profiles:
one letter: Watkins & Walker 1977
two letters: Kristanjansson 1995
Dip of strata
Area of central volcano

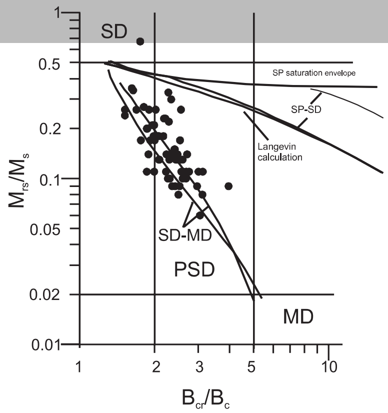

SD
SP saturation envelope
SP-SD
Langevin calculation
SD-MD
PSD
MD
M_{rs}/M_s
B_{cr}/B_c
1
0.5
0.2
0.1
0.05
0.02
0.01
1
2
3
5
10

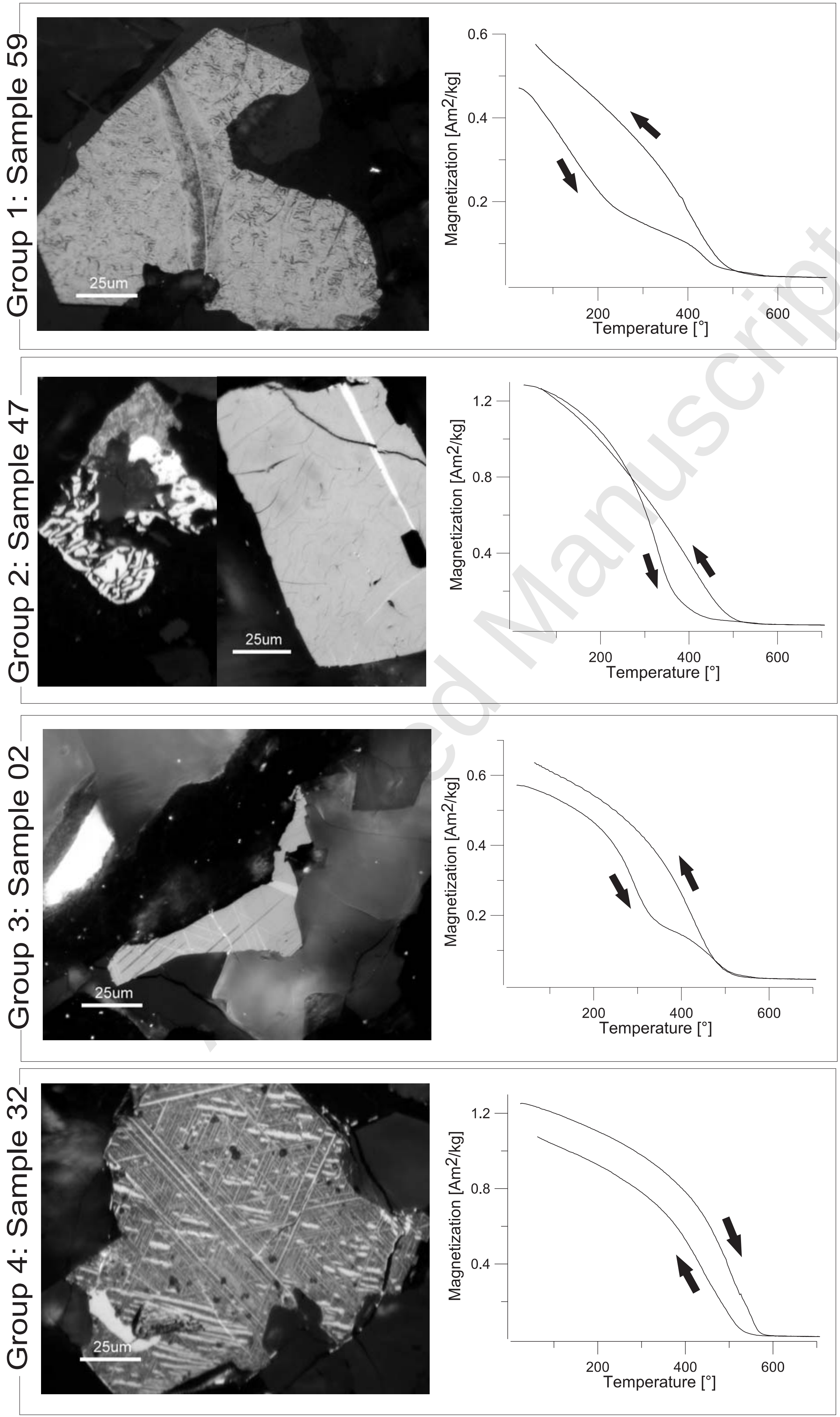
Group 1: Sample 59
25um
Magnetization [Am2/kg]
0.6
0.4
0.2
200
400
600
Temperature [°]
Group 2: Sample 47
25um
Magnetization [Am2/kg]
1.2
0.8
0.4
200
400
600
Temperature [°]
Group 3: Sample 02
25um
Magnetization [Am2/kg]
0.6
0.4
0.2
200
400
600
Temperature [°]
Group 4: Sample 32
25um
Magnetization [Am2/kg]
1.2
0.8
0.4
200
400
600
Temperature [°]

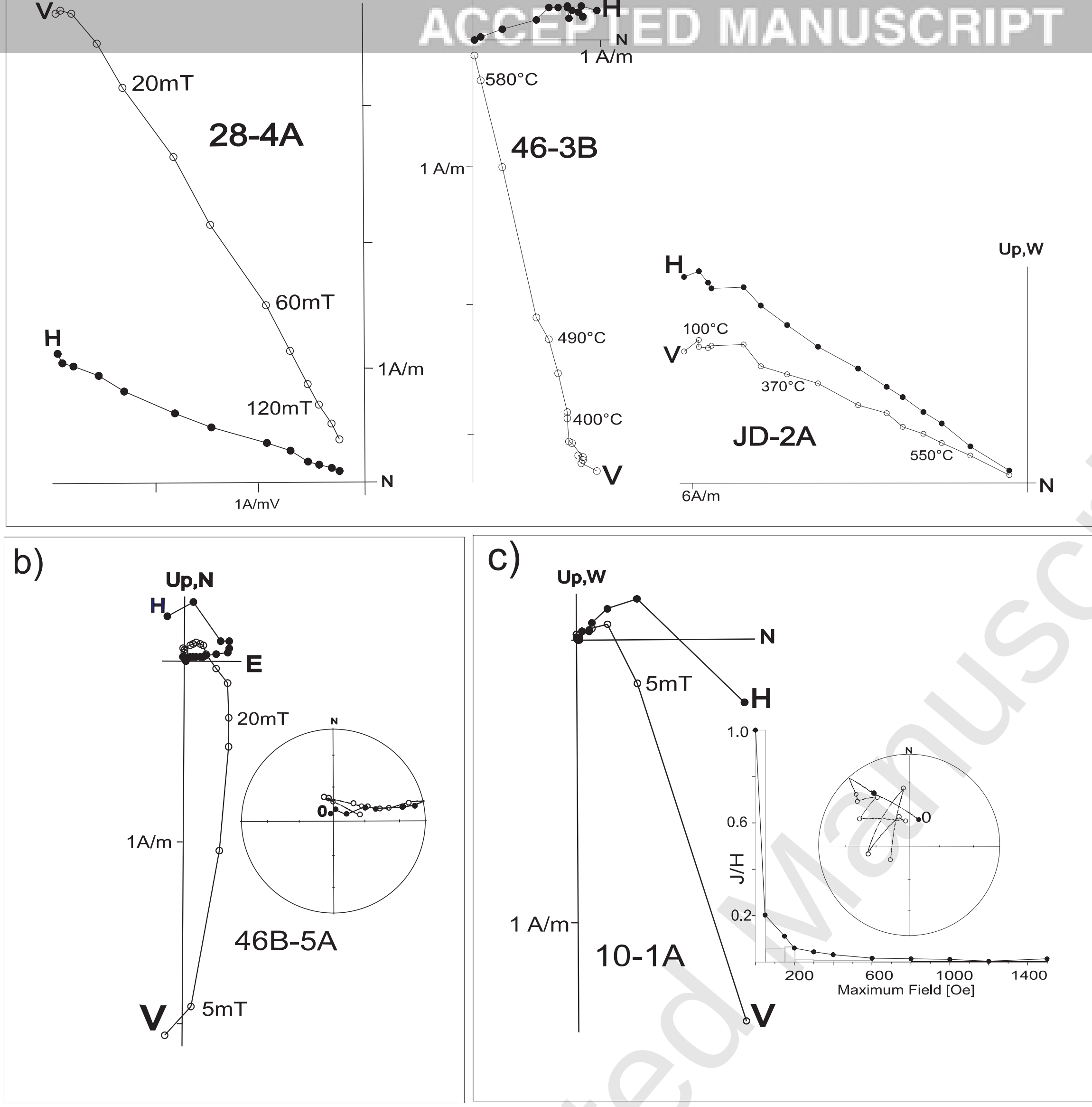
V
20mT
28-4A
60mT
H
1A/m
120mT
N
1A/mV
H
N
1 A/m
580°C
46-3B
1 A/m
490°C
400°C
V
Up,W
H
100°C
V
370°C
JD-2A
550°C
N
6A/m
b)
Up,N
H
E
20mT
N
0
1A/m
46B-5A
V
5mT
c)
Up,W
N
5mT
H
1.0
N
0.6
0
J/H
0.2
1 A/m
10-1A
200
600
1000
1400
Maximum Field [Oe]
V

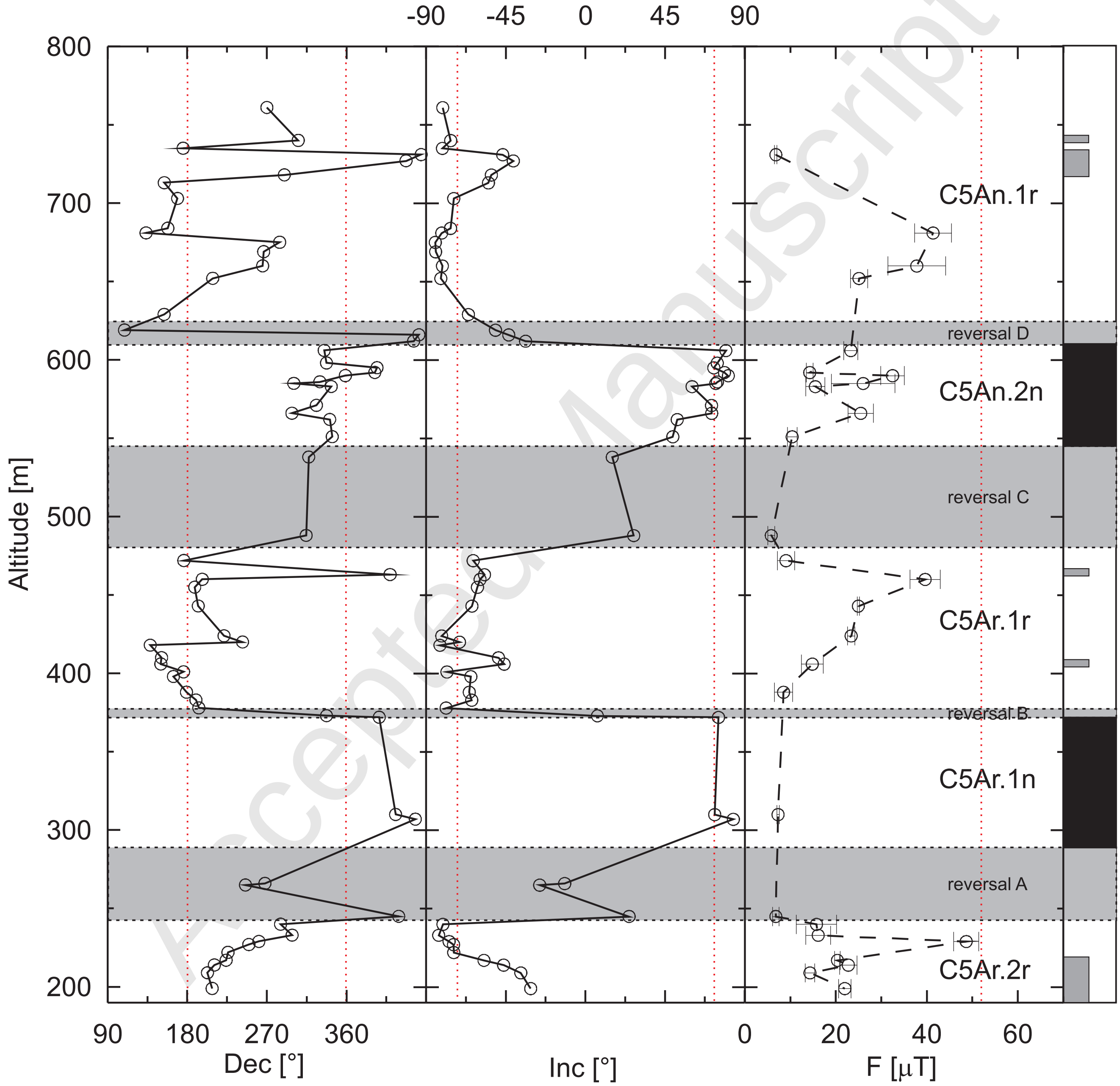
-90
-45
0
45
90
800
700
600
500
400
300
200
Altitude [m]
C5An.1r
reversal D
C5An.2n
reversal C
C5Ar.1r
reversal B
C5Ar.1n
reversal A
C5Ar.2r
90
180
270
360
Dec [°]
Inc [°]
0
20
40
60
F [μT]

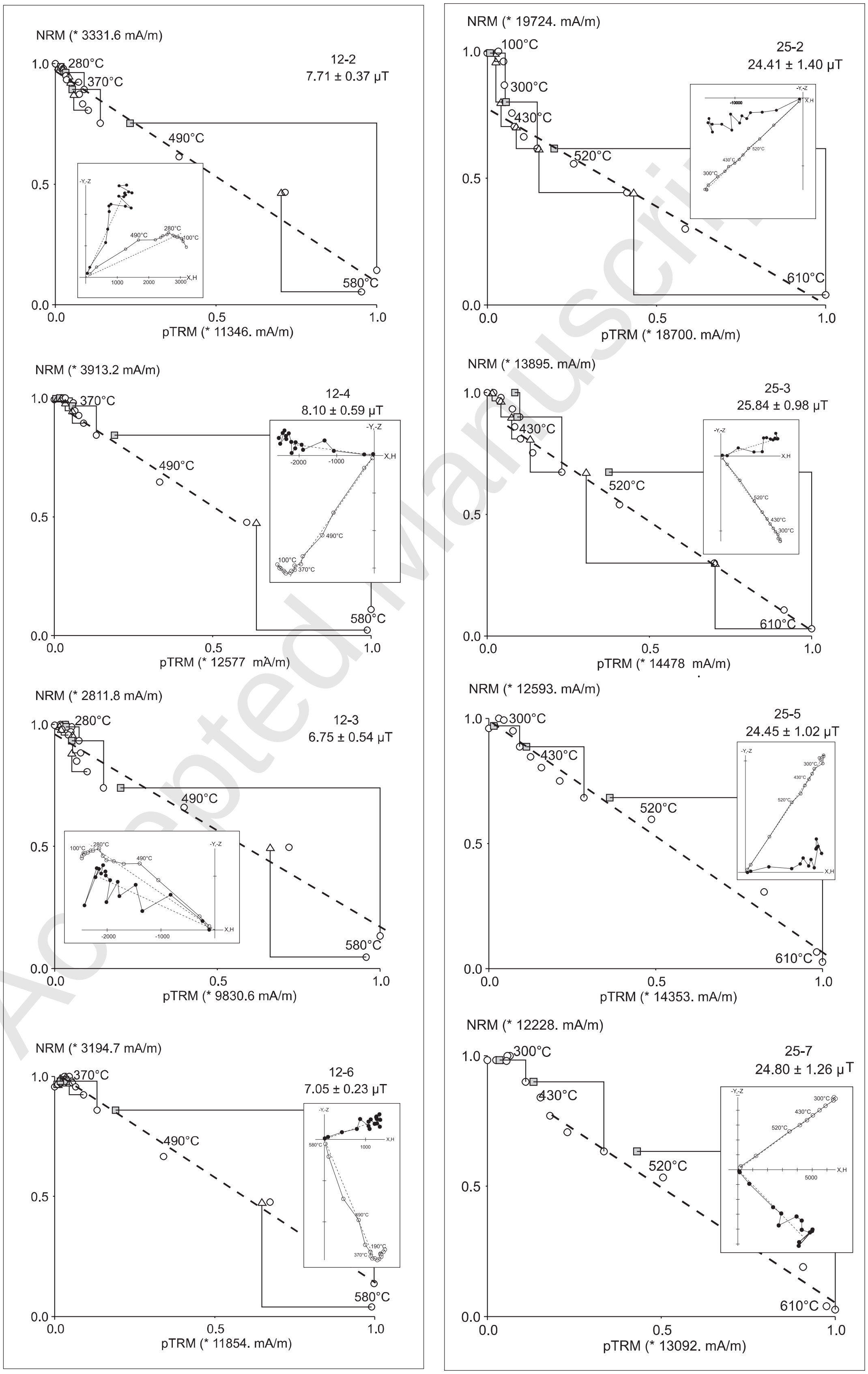
NRM (* 3331.6 mA/m)
12-2
7.71 ± 0.37 μT
280°C
370°C
490°C
580°C
pTRM (* 11346. mA/m)
NRM (* 19724. mA/m)
25-2
24.41 ± 1.40 μT
100°C
300°C
430°C
520°C
610°C
pTRM (* 18700. mA/m)
NRM (* 3913.2 mA/m)
12-4
8.10 ± 0.59 μT
370°C
490°C
580°C
pTRM (* 12577 mA/m)
NRM (* 13895. mA/m)
25-3
25.84 ± 0.98 μT
430°C
520°C
610°C
pTRM (* 14478 mA/m)
NRM (* 2811.8 mA/m)
12-3
6.75 ± 0.54 μT
280°C
490°C
580°C
pTRM (* 9830.6 mA/m)
NRM (* 12593. mA/m)
25-5
24.45 ± 1.02 μT
300°C
430°C
520°C
610°C
pTRM (* 14353. mA/m)
NRM (* 3194.7 mA/m)
12-6
7.05 ± 0.23 μT
370°C
490°C
580°C
pTRM (* 11854. mA/m)
NRM (* 12228. mA/m)
25-7
24.80 ± 1.26 μT
300°C
430°C
520°C
610°C
pTRM (* 13092. mA/m)

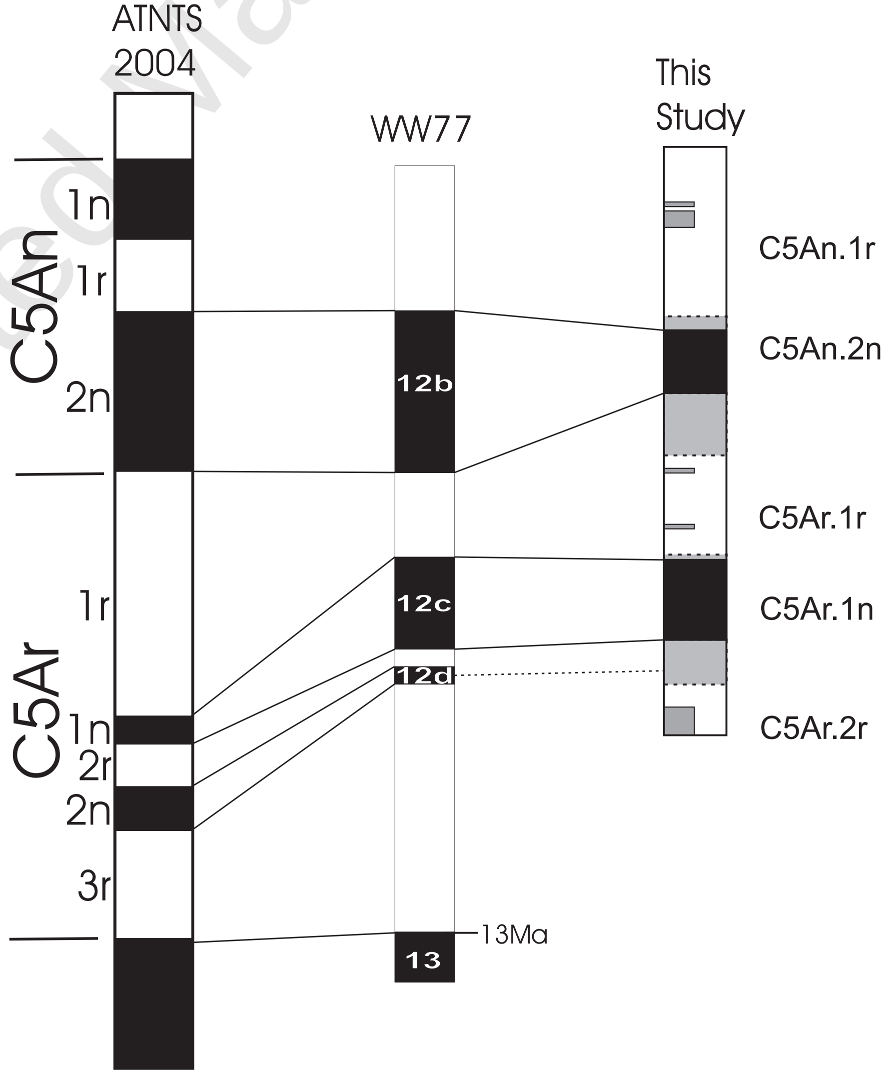

ATNTS
2004
WW77
This
Study
C5An
1n
1r
2n
C5Ar
1r
1n
2r
2n
3r
12b
12c
12d
13
13Ma
C5An.1r
C5An.2n
C5Ar.1r
C5Ar.1n
C5Ar.2r

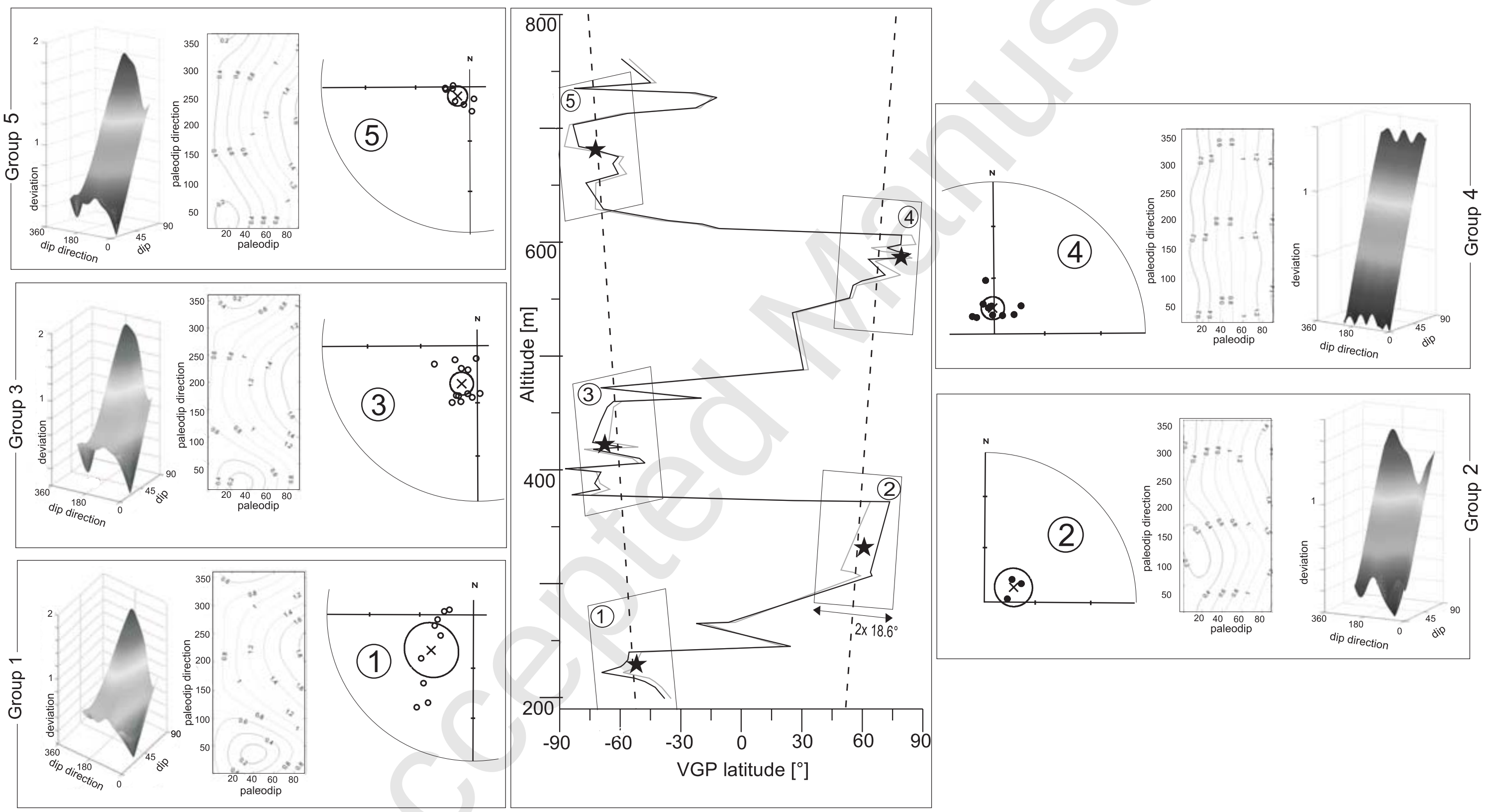

Group 5
Group 3
Group 1
Group 4
Group 2
deviation
dip direction
dip
paleodip direction
paleodip
N
Altitude [m]
VGP latitude [°]
2x 18.6°

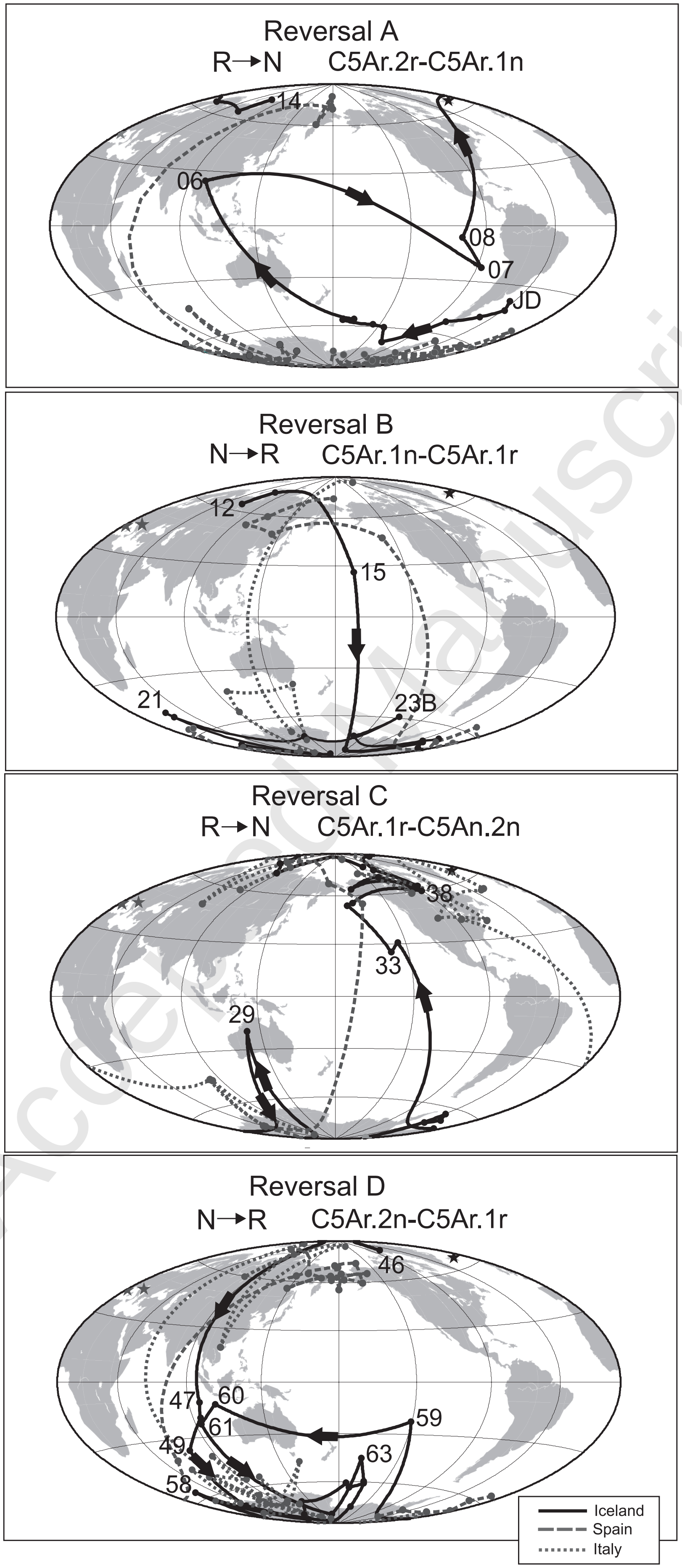
Reversal A
R→N C5Ar.2r-C5Ar.1n
14
06
08
07
JD
Reversal B
N→R C5Ar.1n-C5Ar.1r
12
15
21
23B
Reversal C
R→N C5Ar.1r-C5An.2n
38
33
29
Reversal D
N→R C5Ar.2n-C5Ar.1r
46
47
60
61
59
49
63
58
Iceland
Spain
Italy